Küster, T., Spengler, D., Barczi, J.-F., Segl, K., Hostert, P., Kaufmann, H. (2014): Simulation of Multitemporal and Hyperspectral Vegetation Canopy Bidirectional Reflectance Using Detailed Virtual 3-D Canopy Models. - *IEEE Transactions on Geoscience and Remote Sensing*, *52*, 4, 2096-2108

DOI: 10.1109/TGRS.2013.2258162

Modeling multitemporal and hyperspectral vegetation canopy bidirectional reflectance using detailed virtual 3D canopy models

Abstract

The influence of plant and canopy architecture on canopy bidirectional reflectance and the BRDF is subject of this study. To understand BRDF-influenced reflectance signals, this influence must be identified and quantified, which requires detailed knowledge concerning the structure and BRDF of the observed canopies. BRDF measurements of *in-situ* canopies are time-consuming and depend on the availability of a field goniometer. In contrast to field measurements, computer based simulations of the canopy BRDF offer an alternative approach that considers parameter-driven setups of virtual canopies under constant illumination conditions. This paper presents the *HySimCaR* system, which has been developed in the context of the EnMAP mission. This spectral, spatial and temporal simulation system consists of detailed virtual 3D cereal canopies of different phenological stages, whose geometries are linked to corresponding spectral information. The system enables the simulation of realistic bidirectional reflectance spectra on the basis of virtual 3D scenarios by incorporating any possible viewing position with ray tracing techniques. The parameterization of a number of canopy structure parameters, such as phenological stage, row distance and row orientation, enables the modeling of the bidirectional reflectance and based on them the approximation of the BRDF for many structurally different cereal canopies. *HySimCaR* has been validated with respect to structural and spectral accuracy using three cereal types, including wheat, rye and barley, and 13 different phenological stages. The results show that the virtual cereal canopies are recreated in a realistic way, and it is possible to model their detailed canopy bidirectional reflectance and their BRDF using *HySimCaR*.

1. Introduction

Understanding the influence of plant and canopy structure on canopy bidirectional reflectance is one of the primary tasks of remote sensing. Canopy bidirectional reflectance is determined by the interactions between incoming solar radiation and the plants within the canopy, which depends on the optical and structural properties of the vegetation, the underlying soil and the illumination and viewing geometry. It is important to study these bidirectional effects because several present and upcoming sensors, such as CHRIS (Compact High Resolution Imaging Spectrometer) (Barnsley et al. 2004), RapidEye (http://www.rapideye.com), EnMAP (Environmental Mapping and Analysis Program) (Stuffler et al. 2007, Segl et al. 2012), and PRISMA (PRecursore IperSpettrale of the application mission) (Galeazzi et al. 2008), can observe the same target under different viewing and illumination geometries (possible off-nadir pointing: CHRIS ± 55° in track, RapidEye ± 25° across track, EnMAP ± 30° across track, PRISMA ± 15° across track). This faces enormous challenges in interpreting the acquired data. Furthermore, bidirectional effects due to large pointing angles (>10°-15°, depending on canopy structure) or strongly varying pointing angles (±10°-15°,

depending on canopy structure, multitemporal) lead to uncertainties in the derived remote products, for example the retrieval of vegetation canopy parameters like leaf area index. Therefore, studying bidirectional effects is essential and will contribute to the retrieval of high quality products of future mission data; hence it can increase the accuracy of data products significantly.

Various models can calculate the bidirectional reflectance of vegetation canopies, and they differ predominantly in their ability to model the canopy architecture using one dimensional (1D) or three dimensional (3D) models (Goel 1988). These models can be classified into turbid medium models, simple geometric models, hybrid models and complex geometric models. Models based on turbid mediums (e.g., proSAIL: Jacquemoud et al., 2009, Gao 1993, Myneni et al. 1990, SAIL: Verhoef 1984, Suits 1972) represent the canopy structure by one or several horizontally infinite and homogeneous layers containing statistically distributed, small diffusing and absorbing flat elements representing leaves. Canopy reflectance is calculated solely as a function of leaf density and leaf orientation; in this case, studying the influence of structural properties on canopy reflectance is impossible because the canopy architecture is approximated by only a few parameters. Simple geometric models (e.g., proFLAIR: White et al. 2001, Verbrugghe and Cierniewski 1995, Bégué 1992, Li and Strahler 1986) describe the canopies with simple geometric shapes, such as spheres, cylinders, ellipsoids and cones. These objects, representing plants or sets of plants, are opaque (Verbrugghe and Cierniewski 1995) or porous (Bégué 1992) and cast shadows on the ground and on objects within the scene. The fraction between the illuminated and shaded parts of the scene should explain the major anisotropies of canopy reflectance (Li and Strahler 1986). Hybrid models (e.g., Ni et al. 1999, Gastellu-Etchegorry et al. 1996, Li et al. 1995) are combinations of turbid mediums and simple geometric models where turbid mediums are bounded by simple geometric objects (Li et al. 1995) or in which the scene is represented as a 3D matrix of cells containing turbid materials and facets (DART: Gastellu-Etchegorry et al. 1996,2004). Although these models use 3D structures to approximate canopy architecture, they only consider canopy structures such as row distances and row orientation. In computer simulation models, the canopy architecture is described by detailed 3D plants consisting of numerous small geometric shapes (triangles, cylinders and spheres) (e.g., España et al. 1999, Lewis 1999, Luquet et al. 1998). The canopy reflectance is calculated by computing the outgoing diffuse light intensity of all the surfaces (radiosity models, e.g., Borel et al. 1991) or by tracing the path of photons from the illumination source through the 3D scene up to the observer or vice versa (ray tracing models, e.g., FLIGHT: North 1996, España et al. 1999, drat: Lewis 1999, Rayspread: Widlowski et al. 2006). A realistic description of plant and canopy architecture is essential for achieving accurate simulation results, at least to justify the use of the turbid assumption. Various 3D plant representations have been developed using 3D digitizing methods (Moulia and Sinoquet 1993), photogrammetric techniques (Ivanov et al. 1995) or the silhouette method (España et al. 1999). These models provide very detailed descriptions of plant architecture; however, they are static, meaning that their structure is not able to grow. Prusinkiewicz and Lindenmayer (1990) developed one of the first virtual plant representatives appearing to

be real. This approach was based on L-Systems (Lindenmayer 1968), a formal language mathematically describing the development of biological structures; based on this work, several studies (e.g., Mündermann et al. 2005, Kurth 1994, Goel et al. 1991) have been performed using L-Systems. Beyond the deterministic approach of L-Systems, stochastic models were also developed to generate plant architecture (e.g., Hu and Jaeger 2003, Barczi et al. 1997, Jaeger and de Reffye 1992, de Reffye et al. 1988). These dynamic models offer realistic and detailed descriptions of 3D plant architecture during different stages of plant growth; they become very interesting for remote sensing studies if they are coupled with an appropriate radiation scattering model, particularly for studying the effects of plant and canopy structure on canopy bidirectional reflectance and the bidirectional reflectance distribution function (BRDF).

Such a simulation system comprising a Hyperspectral Simulation of Canopy Reflectance (*HySimCaR*) has been developed in the context of the EnMAP mission and will be presented in this paper. *HySimCaR* enables a spectral, spatial and temporal simulation of bidirectional reflectance and based on them the approximation of the BRDF of different cereal canopies. Cereal canopies are currently of special interest because their cultivation makes up the largest proportion of the world's cultivable land, and agriculture in general is becoming increasingly important due to population growth. The reflectance properties of cereal canopies are subject to interannual variations due to varying chemical composition of the plants and plant organs and the varying geometry of the plants (see *figure 1*). During young phenological stages, the chemical composition of the plants is constant, while the canopy structure changes due to plant growth. After the appearance of the seed heads, the structure of the canopy is stable, while the chemical composition of plants begins to change due to ripening and subsequent senescence. The developed system enables the simulation of all these effects on the basis of virtual 3D scenarios coupled with Monte-Carlo ray tracing techniques that incorporate all possible viewing geometries. The interpolation of different observations results in the approximation of the BRDF. The study was performed for 3 different cereal types: winter wheat (*Triticum aestivum*), winter rye (*Secale cereale*) and winter barley (*Hordeum vulgare*) at 13 different phenological stages.

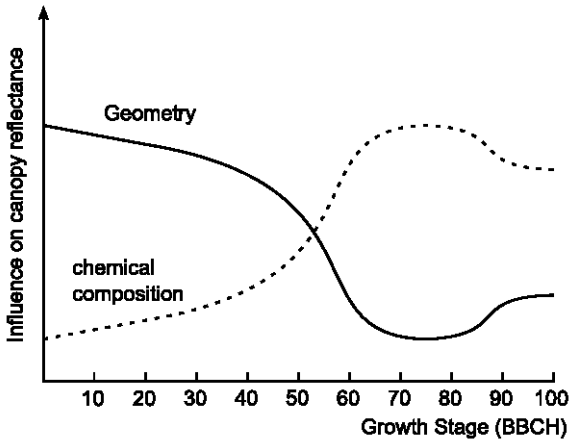

Figure 1. Influencing role of chemical composition and geometry of plants on canopy reflectance.

2. Simulation of top-of-canopy reflectance

This section describes the simulation of the top-of-canopy bidirectional reflectance of cereal canopies. First, the build-up of virtual 3D cereal plants is presented including the capture and pre-processing of the relevant data. Second, soil digital elevation models (DEMs) were developed. Each soil DEM was superposed with numerous cloned plant representatives describing one virtual 3D cereal canopy. Third, the simulation of bidirectional canopy reflectance of the developed 3D virtual cereal canopies using Monte-Carlo ray tracing techniques is described.

2.1 Plant and canopy data

Two study sites in eastern Germany were chosen for the data capture. The Berlin-Dahlem site is a long-standing testing ground of the Faculty of Agriculture and Horticulture of the Humboldt University of Berlin. The other site, Beelitz-Wittbrietzen, is a typical agricultural landscape in eastern Germany characterized by the cultivation of different crops close together and is well suited for monitoring plant development and taking measurements regularly. Both test sites were sampled in nearly regular intervals during the 2006/2007, 2007/2008 and 2008/2009 growing seasons. Spectral measurements and measurements of the plant and canopy architecture were sampled for the 3 selected cereal types.

2.1.1 Spectral information

The spectral reflectance measurements were collected using an ASD FieldSpec Pro FR spectroradiometer, which records the electromagnetic radiation reflected by the target from 350 nm – 2500 nm in 2151 spectral bands featuring a spectral resolution of 3 nm (350 nm – 1000 nm) and 10 nm (1001 nm – 2500 nm) interpolated to 1 nm. All the spectral measurements were collected under clear skies between 2 h before and after the sun meridian to ensure likewise illumination conditions with an 8° foreoptic. The canopy reflectance was measured approximately 1 m above the plants (diameter of field of view about 14 cm) in the nadir direction while walking slowly through the canopy and integrating a spectral signal (average of 20 x 50 individual ASD measurements). Several transects (about 20 m) were sampled in this way to obtain representative spectra for each canopy at each growth stage. Numerous reflectance measurements of leaves, culms and seed heads were taken approximately 5 cm above the plant organ while using a dark standard background to prevent transmission effects. Proved as most suitable, a kind of black craft foam was used as background due to its low reflectance of about 4 % in the relevant wavelength range. For each target, 10 spectral measurements (each averaged of 50 individual ASD measurements) were taken and averaged to minimize noise and the inherent variability of the plants and to average out variances due to the measurement method.

The spectra were stored in spectral libraries and corrected for detector jumps (offset between two detectors). Bands in the spectral ranges between 1350 nm – 1420 nm, 1820 nm – 1940 nm and 2450 nm – 2500 nm were masked and ignored in the

simulation process due to their low signal-to-noise-ratios (SNRs) caused by strong water vapor absorption in the atmosphere.

Unfortunately, it was not possible to measure the single-path transmittance of leaves. Hence, leaf transmittance was estimated from the measured leaf reflectance data using PROSPECT5 (Féret et al. 2008, Jacquemoud and Baret 1990) for vital green leaves and PROSPECT with a specific absorption coefficient for brown pigments (Frédéric Baret, personal communication 2009) in dry leaves. A database of PROSPECT leaf reflectance and transmittance data comprising all the possible combinations of constituents was generated. A cost function between the measured leaf reflectance R_{mea} and the modeled leaf reflectance R_{mod} was used to estimate the appropriate transmittance spectrum. The cost function C_{LSN} (*equation (1)*) is a variation of the least square function calculating the squared distance between the measured and modeled reflectance spectra over all of the spectral bands n_b normalized by the measured reflectance (least square normalized cost function). Hence, no spectral band is favored with respect to another band (Bacour 2001). For each measured leaf reflectance spectrum, the cost values for all the modeled reflectance spectra were calculated. The minimum of these values indicates the most similar reflectance spectrum whose associated transmittance spectrum was selected for use.

$$C_{LSN} = \sum_{i=1}^{n_b} \left(\frac{R_{mea_i} - R_{mod_i}}{R_{mea_i} + R_{mod_i}} \right)^2 \quad (1)$$

2.1.2 Geometrical information

The geometrical information of the plant and the canopy architecture were collected manually. Each plant structure element was measured numerous times on different plants to obtain characteristic values for each structural element. The following elements were measured (see also *figure 2*): the number of tillers per plant; the number of leaves per tiller; the number of internodes (part of the tiller between two leaves) per tiller; the length of each internode depending on the tiller order (in regard to the order of appearance); the diameter of each internode; the length and width of each leaf depending on the tiller order (in regard to the order of appearance); the angle between the leaf and the tiller; the length and diameter of the seed head; and the length of the awns.

The canopy architecture was determined by the plants and their arrangement in the underlying soil. The soil has characteristic furrows in approximately equal distances (between 13 cm and 17 cm), which are due to the mechanical drilling of seed. This soil geometry was measured by collecting the height profiles.

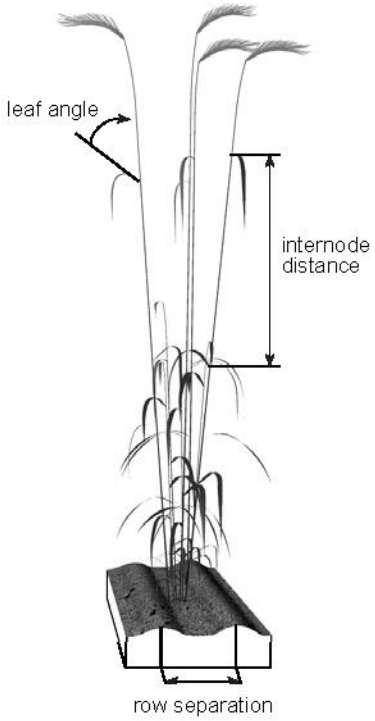

Figure 2. Rye plant on underlying soil with selected model parameters.

2.1.3 Plant development

Besides the numeric measurements, the development of the different plant parts during growth was observed.

Tillering: When the fourth leaf of the cereal plant emerges from the main stem, new tillers sprout out of the bottom of the main stem. From this point on, every time the main stem grows an additional leaf, it will also produce a new tiller until tillering is complete. The number of produced tillers varies depending on several factors, such as canopy density, sowing date, mineral nutrition and the use of plant growth regulators. Only some of the produced tillers will survive, and the remaining tillers will die mainly due to competition for resources such as light and nutrients (Kirby 2002).

Torsion and Bending of leaves during growth: The leaves start twisting through their longitudinal axis after their appearance. Bending is forced by the leaf weight while simultaneously reducing the former twist during leaf development.

Bending of stems during ripening: The stems are flexible elements capable of bending from the weight of peripheral plant parts such as the leaves and seed head; specifically, the weight of seed heads increase during fruit development, leading to the bending of the last internode of the tillers.

Bending of seed heads during ripening: The main axis of the seed head loses its resilience, and the seed head bends under its own weight when senescence starts.

2.2 Plant models

The accuracy of the results from the computer simulation models strongly depends on the 3D representatives, i.e. mockups. The 3D plant representatives used for this study were generated by *AmapSim* (Barczi et al. 2008, 1997), scientific software based on the AMAP (botAnique et bioinforMatique de l'Architecture des Plantes) framework of de Reffye et al. (1988), which provides stochastic rules for the description of plant growth and development. The fourth dimension is introduced by the growth engine, which is the core of the software and describes the evolution of the plant organ number, organ size, and organ position as time progresses. This engine is based on botanical theory to simulate plant morphogenesis and organogenesis (Barczi et al. 2008), which produces detailed 3D plant architectures of the aerial parts of plants at different stages of plant growth assuming typical growing conditions. Limited water or nutrients scenarios as well as influences of neighboring plants will not be considered. *AmapSim* enables the modeling of numerous different plant species by calibrating parameter values; therefore, it is relevant to a wide range of users. Some examples of its applications include sunflower (Rey et al. 2008, Dosio et al. 2003), maize (Yan et al. 2004), black pine (Castel et al. 2001) and coconut (Mialet-Serra et al. 2001). AmapSim plant models have also been used to simulate canopy reflectance. For example, Dauzat and Hautecoeur (1991) modeled a millet canopy to simulate bidirectional reflectance using Monte-Carlo ray tracing techniques.

2.2.1 Topology

The structural build-up of an *AmapSim* plant model is driven by the physiological ages that define the modeling of plant components. *Figure 3* illustrates the chosen topology (i.e., relative position of the plant components) for a barley and a rye plant (the seed head of wheat plants has no awns and has a physiological age of 2001). The plant model is classified into the following plant organs and associated physiological ages: root (physiological age 1-9); tillers (physiological age 11-89); leaves (physiological age 101-801); and the seed head (physiological age 1001-2001).

The plant model includes a root system that will not be displayed in the 3D representation, but it is necessary for the arrangement of tillers. The model consists of several tillers (maximum 8). Each tiller is divided into nine internodes (e.g., for tiller 1, physiological age 11-19; for tiller 2, physiological age 21-29; etc.), and each internode is subdivided into 10 segments (see *figure 3* at physiological age 19). Each tiller develops a leaf at the top of each internode and a seed head at the top of the last internode. Every leaf is defined by a single physiological age and is subdivided into 100 segments. The seed head is divided into 30 segments, with each segment associated with 2 awns. The subdivision into segments allows for better a geometrical description of complex behavior during the growth of specific plant elements, e.g., the torsion and bending of leaves, the bending of tillers, and the bending of seed heads (cf. *section 2.1.3*).

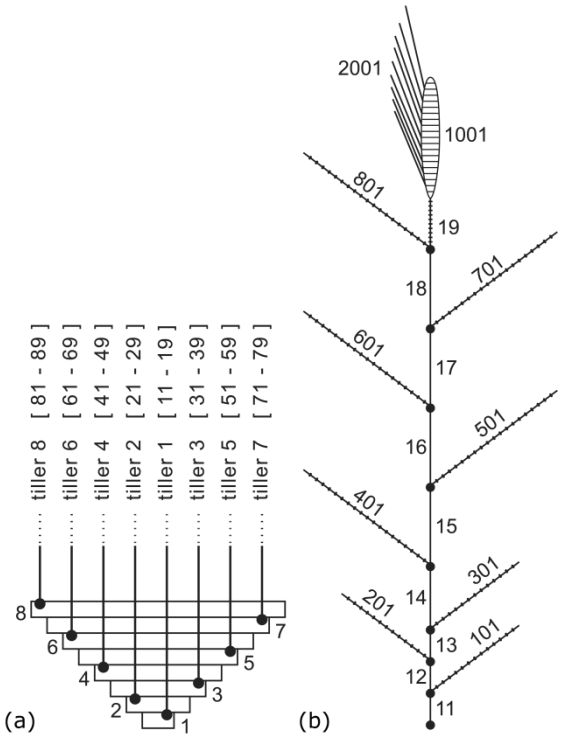

Figure 3. Topology of a rye/barley plant developed for use in *AmapSim*: (a) root system; (b) aerial parts of the plant. The numbers depict the physiological age of the plant elements.

2.2.2 Geometry and growth

Each plant element and segment is linked with 3D geometrical objects. The physiological ages linked to the internodes, seed heads, and awns are represented by cylinders, the physiological ages linked to the leaves by polygon surfaces (facets). To achieve a realistic 3D plant representative, the specified shapes were placed in the 3D space using accurate geometrical rules. The bending and straightening of axes is defined by their material elastic properties, i.e., the shape of an axis bends under simulated self-weight (cf. Barczi et al. 2008, 1997).

Growth is modeled through the size variations of the model elements. Each defined model element is specified by an initial length and diameter at its birth. Based on an initial time and a specified increase coefficient, the size grows within a defined time period. Size variation with *AmapSim* is only modellable in one direction (growing or shrinking); thus, the shrinking of leaves due to senescence after reaching maturity is not possible. Moreover, the modeling of the torsion and bending of leaves and the bending of seed heads are not accurate using the default *AmapSim* functionalities. For these reasons, two external plug-in modules of *AmapSim* were developed to improve seed head bending, the simulation of leaf size and the bending and torsion of leaves over time. These modules successively allow the rotation (in the case of torsion) or stacking (in the case of bending) of the geometric objects in the 3D space. Each variation is defined by a starting time and a preceding time period. Depending on the type of variation, additional parameters must be set (e.g., the size ratio, the bending

angle, the active bending section of the leaf or seed head, the torsion angle, and the active torsion section of the leaf). *Figure 4* shows the modeled plant representatives for the three cereal types at the selected phenological stages.

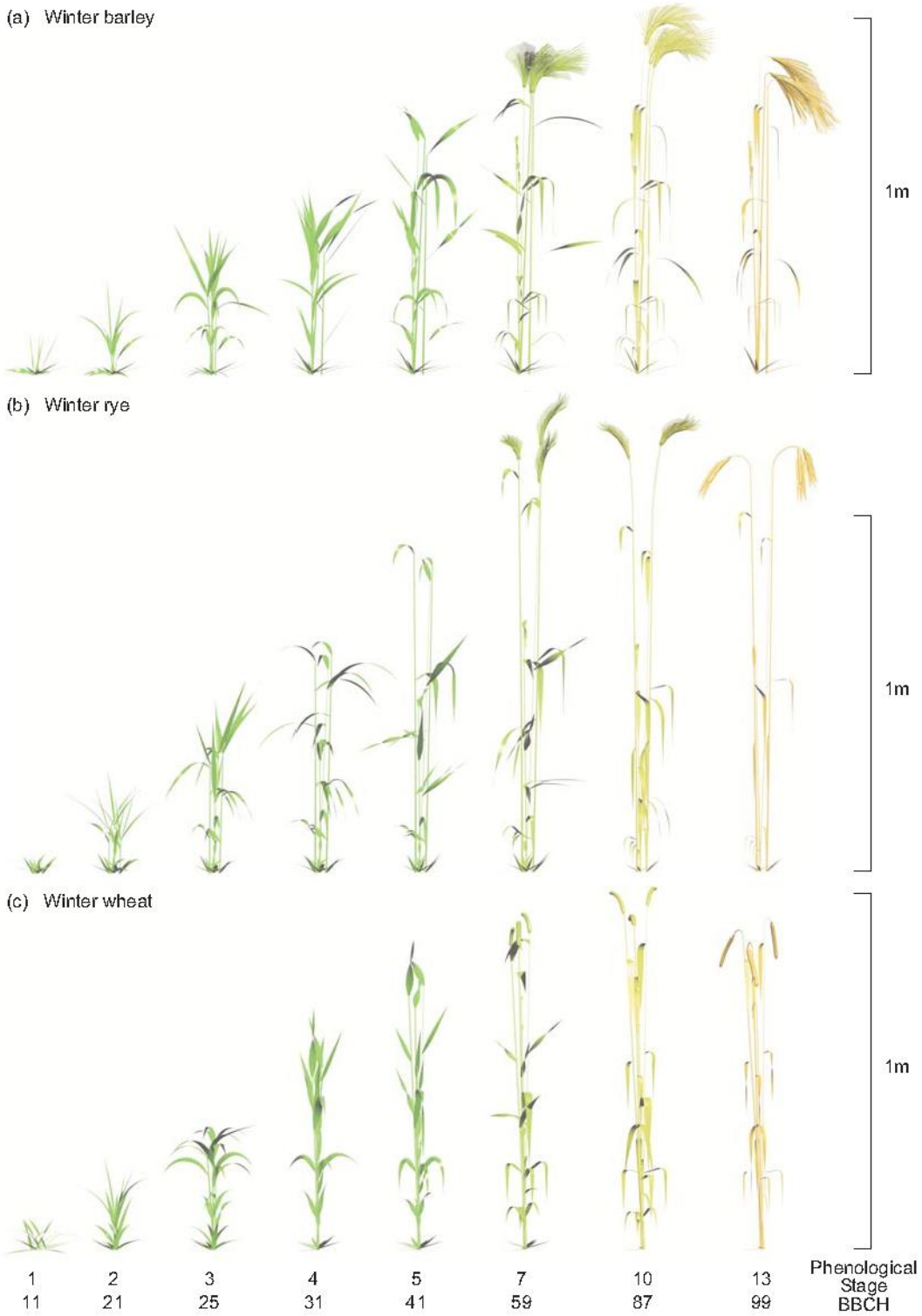

Figure 4. Plant mockups of (a) winter barley, (b) winter rye and (c) winter wheat at selected phenological stages. Colors are not real.

2.3 Soil model

A database of field-measured height profiles was created and used to generate a digital elevation model (DEM) of the soil. By defining the extent and row orientation of the scene, a set of height profiles varying in width were chosen from the database and used to form a template pattern. The template was shifted along the row orientation to estimate the DEM values. Furthermore, the DEM was overlaid by granular patterns to achieve a natural structure. Each pattern is represented by a half sphere with variable size, opens either upwards or downwards and is randomly placed within the DEM (Kuester 2011).

2.4 Canopy model

A virtual 3D canopy is composed of several 3D plant mockups and a soil DEM. First, the 3D plant mockups must be linked with the reflectance and transmittance characteristics. Therefore, all the segments of a phytoelement (e.g., a leaf or an internode) are grouped. Each group is linked with one type of spectral information chosen from the spectral database. For each phytoelement at each phenological stage, several spectra were randomly chosen (ensuring spectral variations within the canopy) and stored in the database. The BRDF model of all phytoelements is assumed as Lambertian reflectance. This assumption is adequate for culms, seed heads and grains because their cylindrical shape ensures uniform scattering and for the leaves because of their dull surface.

The positioning of the plant mockups on the soil DEM must consider the row distance and seed density, which affect the typical row structure and plant density. First, the plants are arranged regularly along the center of the furrows using a predefined linear density along the row. Second, each plant is shifted randomly along and across the row following a Gaussian distribution to ensure a natural composition. The complete virtual 3D canopy contains several plant mockups, which are prototypes. These prototypes differ in their physiological and morphological development (number of tillers, number of depauperate tillers) and represent plants of a single specific phenological stage. Each clone is randomly chosen from the set of possible prototypes and randomly rotated around its vertical axis to ensure a natural composition and to avoid continuous patterns that could cause aliasing effects. In summarizing the generation of a virtual 3D canopy (for instance, in *figure 5* for a canopy during late stem elongation), the following parameters were found to be relevant: row distance (RD); row orientation relative to the sun azimuth angle (RRO); the number of plants per meter of row (PPM); and the number of vital and depauperate tillers (TPP). Additionally, it is possible to estimate the leaf area index (LAI) and the percentage cover (PC) of each virtual 3D canopy after generation. For the LAI, the one-sided area of all the facets shaping the leaves are summed for each plant prototype and multiplied by the number of clones within the canopy model. The LAI is then calculated by normalizing the total sum of leaf area with the horizontal area covered by the canopy (LAI definition according to Monteith (1973)) in contrast to the LAI measurements in the field, where the LAI is often estimated indirectly through radiation measurements or through

hemispherical image analysis, while keeping time and effort of the field measurements to a minimum (Bréda 2003). For the estimation of the PC, the virtual 3D canopy is mapped in the horizontal plane using an orthographic projection. The PC was then calculated by normalizing the number of vegetation pixels according to the total number of pixels in the mapped image.

Figure 5. Virtual winter rye canopy during late stem elongation (BBCH 41, phenological stage 5). Image generated with *drat*. RGB stack of R = 670 nm, G = 550 nm and B = 460 nm.

2.5 Canopy reflectance simulation

In this study, the canopy reflectance was calculated using the aDvanced Radiometric rAy Tracer (*drat*), an efficient Monte-Carlo ray tracing renderer developed by Lewis (1999). Ray tracing is used in the computer graphics community to produce 2D images of defined 3D geometric models by tracing the path of light through the 3D scene (Glassner 1989); in the imaging spectrometry field, it is used for reflectance computations using forward or reverse ray tracing techniques. Photons are fired from an illumination source, trace their way through the scene and are collected by a sensing element (e.g., camera), thereby simulating the effects of their encounters (reflectance, absorptance or transmittance) with the scene objects (forward ray tracing). If an encounter occurs, the probability of reflectance, absorptance or transmittance is determined by the object material decided for each encounter (Glassner 1989). Because a large portion of light does not reach the sensing element, it is much more computationally efficient when the simulation is conducted in the direction of the sensor (reverse ray tracing), which is the method implemented in *drat*. Furthermore, *drat* uses a special ray tracing technique, the Monte-Carlo method, which enables the implementation of diffuse interactions of light between the objects and is of high interest for vegetation canopies (volume scattering). The *drat* model has been used in numerous simulation studies (e.g., Disney et al. 2006, 2000, Saich et al. 2003, 2002, Widlowski et al. 2007) and has been shown to fit with both field measurements and other models simulating the canopy radiation regime. Furthermore, *drat* participated on the RAdiation transfer Model Intercomparison (RAMI), whose primary objective was the documentation of the differences between canopy reflectance models under well controlled experimental conditions (Pinty et al. 2001). The comparison especially for

heterogeneous 3D scenes resulted in deviations of only 1-3 % of their BRF values of six, among them *drat*, of the participated 3D Monte-Carlo ray tracing models. Since the third phase of RAMI (RAMI-3, Widlowski et al. 2007) the *drat* model belongs to a series of "credible" 3D Monte-Carlo ray tracing models. The others are *DART* (Gastellu-Etchegorry et al. 1996,2004), *FLIGHT* (North 1996), *Rayspread* (Widlowski et al. 2006), *raytran* (Govaerts and Verstraete 1998), and *Sprint3* (Thompson and Goel 1998), (Widlowski et al. 2007).

Several camera models are implemented in the *drat* software (e.g., a planar camera model and a spherical camera model). We used the planar camera model, which is the most commonly used camera model capable of recording by central perspective or orthographic methods. We used the orthographic method assuming the theoretical case of parallel directional pointing for each pixel, i.e. for each *drat* calculation. Defining the camera model requires a viewing position (specified by the azimuth and zenith angles), a viewing direction (specified by looking at the point and boom length), and an observing area (specified by a field of view or an ideal observation of the area). We found out, that the resulting canopy spectrum of the same 3D canopy varies insignificant integrating a canopy scene over 1 m by 1 m or 5 m by 5 m or 20 m by 20 m. We also found out, that the 3D canopy has to be much greater sized than the sampled area to include the adjacent scattering that is important to obtain the volume scattering of the canopy. Hence, the modeled canopies are 3.5 m by 3.5 m sized to observe an area of 1 m by 1 m in the center. For bidirectional reflectance simulations, conform to case 1 after Nicodemus et al. (1977) and Schaepman-Strub et al. (2006), a directional illumination source is used by specifying the azimuth and zenith angles. In summary, the bidirectional reflectance factor (BRF) of a given 3D vegetation scene under a given observation and illumination constellation is modeled as the result of a *drat* calculation.

3. Results and discussion

3.1 Bidirectional reflectance

Bidirectional canopy reflectance spectra of the three cereal types at 13 different phenological stages (11 – 99 after BBCH scale system of BBCH) were calculated for the nadir observation position. Therefore, numerous different canopies varying in plant appearance and plant density were sampled (cf. section 2.1.1). Plant density is driven by the row distance, the number of plants per meter, and the number of tillers per plant (vital and depauperate). The row distance varied between 13 cm and 17 cm, representing values measured in the test site. The values chosen for the number of plants per meter were between 8 and 16, and the values chosen for the number of tillers per plant were between 2 and 6 (each with 2 or 3 vital tillers). Every canopy composition was built using several plant prototypes, where the following 4 different lists of prototypes were used: prototypes with 2, 3, and 4 tillers in total; prototypes with 2, 3, 4, and 5 tillers in total; prototypes with 3, 4, and 5 tillers in total; and prototypes with 3, 4, 5, and 6 tillers in total. Row orientation, which is measured relative to the sun azimuth

angle and sun position, was adapted to the field conditions, but with ±10° and ±20°, respectively. In summary, 144 different canopy set-ups were built for each phenological stage and each cereal type. In total, the following 31 different cases were modeled due to the availability of the field-measured data: 11 phenological stages for winter barley, 13 phenological stages for winter rye, and 7 phenological stages for winter wheat. These measurements comprise a total of 4464 reflectance calculations.

3.1.1 Spectral validation

The pairs with the best fits were determined between field-measured and modeled canopy reflectance spectra. Therefore, a cost function using a least squares analysis was minimized in addition to the derivation of the transmittance of the leaves (cf. *equation (1)*). The comparison was made for each cereal type and phenological stage separately, and this comparison was performed once for the unchanged original spectra and once for the previously normalized (division of all the bands by the highest spectral band value of the spectrum) spectra. Normalizing the spectra eliminates differences caused by albedo variations and is necessary to consider the shape of each spectrum.

For 17 of the 31 analyzed cases, good and very good agreements were obtained for shape and overall albedo. A total of 12 other cases resulted in good and very good agreements (cf. *figure 6*) in shape, but differed in their overall albedo. Moderate agreements were obtained in shape for only 2 cases, but these 2 cases had good agreements in their overall albedo. *Table 1* summarizes the results.

Table 1. Comparison of results between field-measured and simulated canopy reflectance: ++ very good agreements in shape and albedo; + good agreements in shape and albedo; ** very good agreements in shape but not in albedo ; * good agreements in shape but not in albedo; – moderate agreements in shape but good in albedo.

Phenological Stage No.	BBCH	Winter Barley	Winter Rye	Winter Wheat
1	11	++	+	no val. data
2	21	*	*	no val. data
3	25	+	–	no val. data
4	31	++	++	++
5	41	++	+	++
6	51	*	**	no val. data
7	55-59	*	**	++
8	71	*	**	no val. data
9	81-85	*	++	++
10	87-89	+	+	*
11	91	*	+	+
12	95	no val. data	*	no val. data
13	99	no val. data	+	–

The less than good agreements may have been caused by several factors. For example, different soil moisture contents lead to different overall albedos. All the simulations

were performed with a soil spectrum containing soil moisture of 4 vol%. Measuring canopies with a drier soil would lead to a spectrum with a higher overall albedo. Furthermore, the spectral input of the simulation determines the result of the modeled canopy spectra. Leaf surface reflectance is also angle dependent and is difficult to respect while measuring in the field. Thus, in general, too low leaf reflectance leads to too low canopy reflectance, which occurred in 12 of the 31 analyzed cases (cf. *figure 6 (c)* and *(d)*). In the senescence phenological stages, the presence of vital understorey vegetation affects the vital reflectance spectra, which was not included in the simulation but occurred in the field (cf. *figure 6 (e)*).

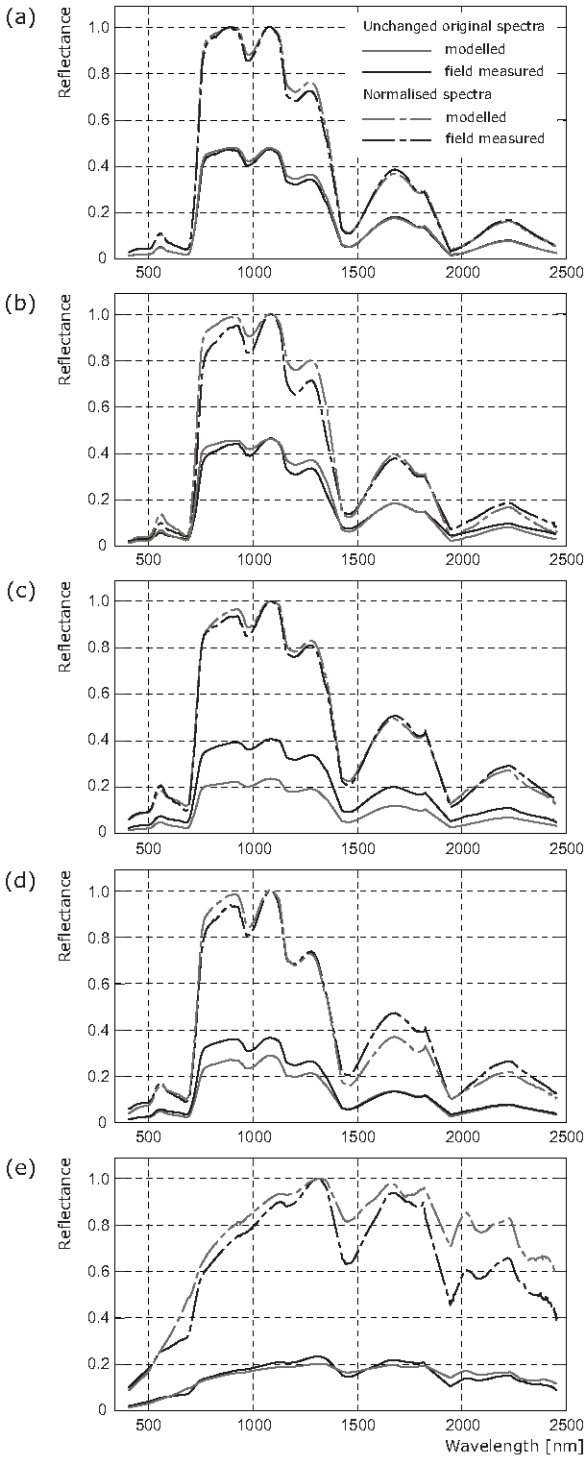

Figure 6. Examples for the different categories of agreements: (a) very good agreements in shape and albedo; (b) good agreements in shape and albedo; (c) very good agreements in shape but not in albedo ; (d) good agreements in shape but not in albedo; (e) moderate agreements in shape and albedo.

3.1.2 Structural validation

The PCs of the spectrally best-fit scenes were compared to validate the structure of the modeled canopies for the three cereal types and the 13 phenological stages. First, the PC of the *in-situ* canopies was estimated using photos taken in the field during the different phenological stages. Each photo was taken with a frame of 0.5 m by 0.5 m by measuring equal-sized areas. The pixels were classified into specific vegetation and soil background categories using a classification tree. First, green vital vegetation was separated if the green band signal G was higher than the red band signal R. Second, dark (mostly shadowed) soil was separated from dry vegetation using the total albedo of all three signals (R+G+B). The separation of light (mostly illuminated) soil and dry vegetation is barely possible; however, because areas with illuminated soil occur rarely in senescence phenological stages, this error is tolerable. The PC is then given by the number of vital and dry vegetation pixels normalized by the total number of pixels of the photo. In contrast, the PC of the virtual canopies was calculated as described in *section 2.4*.

Figure 7 visualizes the comparison of the PC of the spectrally best fitting scenes. The values of winter barley and winter rye show good agreements for all the analyzed phenological stages. Even the moving average curves of both the modeled and *in-situ* canopies show a good fit. For winter wheat, the values of the PC of modeled canopies were distinctly below the values of the *in-situ* canopies. However, the distribution of the values resembles the distribution of the values of winter barley and winter rye. The curve of the winter wheat *in-situ* canopies forms nearly a straight line. Thus, the values of the *in-situ* canopies do not appear to be representative; one reason for this finding is probably due to the presence of vital understorey vegetation, that were observed in the *in-situ* canopies during the field campaigns, resulting in a high PC. Anyway, the PC is a strong parameter to indicate canopy structural changes during the growing season. Thus it is not surprising that the comparison between the PC curves and the geometry line in *figure 1* reveals a strong relationship between both. The geometry line can be found as the changes of the PC per time unit describing a measure of the influence on canopy reflectance.

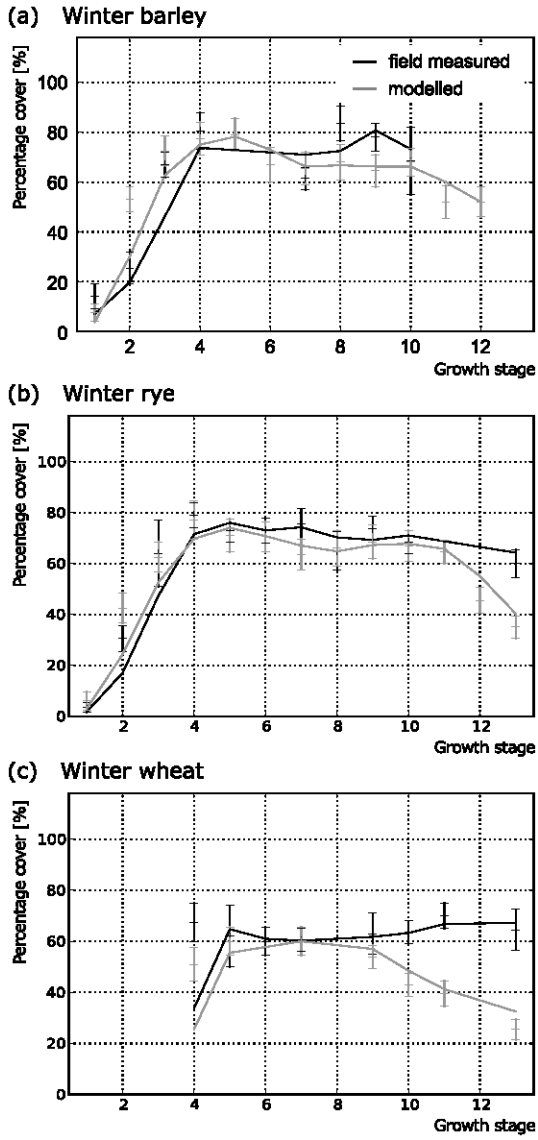

Figure 7. Comparison of PC of *in-situ* and modeled canopies for (a) winter barley, (b) winter rye, and (c) winter wheat. The markers show the mean value and the ± standard deviation for each phenological stage. The graph represents the moving average (kernel size three, repeating values at the edge) of the mean values.

In addition, the LAI of the spectrally best fitting scenes was investigated to obtain a three-dimensional impression of the canopy structure. The LAI of the virtual canopies was calculated as described in *section 2.4*. Due to the absence of comparative field measurements, the LAI data of cereal canopies during their phenological development were researched in the literature to make an approximate assertion. *Figure 8* visualizes the LAI values of the spectrally best-fit scenes. A typical seasonal curve with its maximum before the start of ripening was found for all three species, which has also been described in the literature (e.g., Kanemasu 1974, Zhang et al. 2004 and Baghestani et al. 2006).

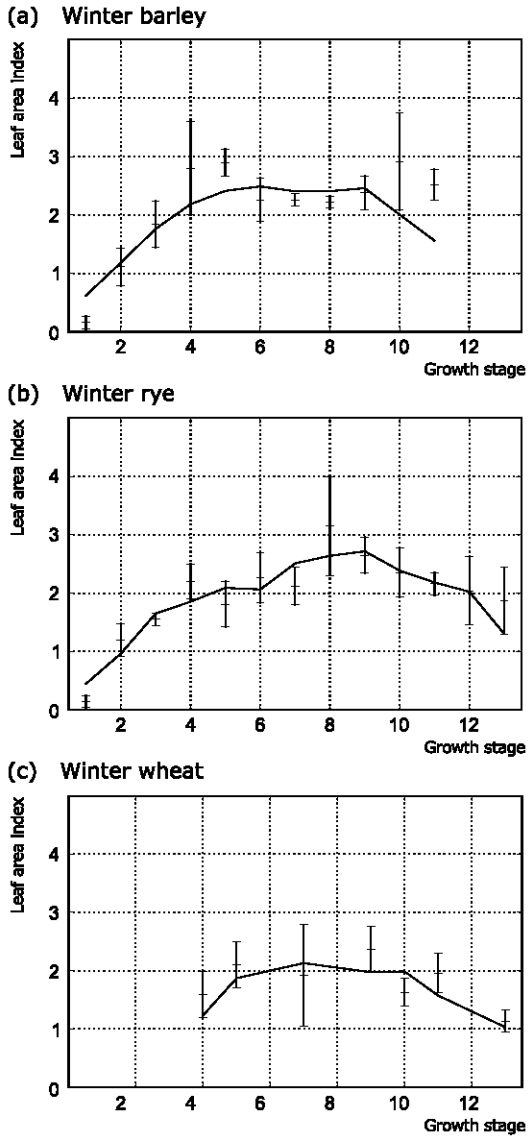

Figure 8. LAI values of virtual canopies for (a) winter barley, (b) winter rye, and (c) winter wheat. The markers show the mean value and the ± standard deviation for each phenological stage. The graph represents the moving average (kernel size three, repeating values at the edge) of the mean values.

3.2 Bidirectional reflectance distribution function

The previous studies demonstrated that realistic cereal canopies can be modeled. This enables the approximation of the BRDF of these cereal canopies because *drat* is capable to calculate the BRF of any viewing position of the observation hemisphere. The interpolation of these different observations results in the approximation of the BRDF.

Each modeled canopy is sampled from 113 different viewing positions of the hemisphere for zenith angles between 0° and 65° (see *figure 9*). Observations with larger zenith angles are of less importance for remote sensing applications. The selected observation positions were chosen to be non-uniformly distributed. This prevents disturbing patterns caused by the interpolation process in order to visualize the BRDF.

The principal and the cross plane are observed in fine and regular intervals (each 5°) because these parts are of higher interest of the BRDF model. Interpolation is performed by fitting a surface of the form z = f(x,y) to the sampled data vectors (x(θ_r, ϕ_r), y(θ_r, ϕ_r), z), where z = (θ_i, ϕ_i, θ_r, ϕ_r) is represented by the bidirectional reflectance factor observed from the position (θ_r, ϕ_r) and illuminated from (θ_i, ϕ_i).

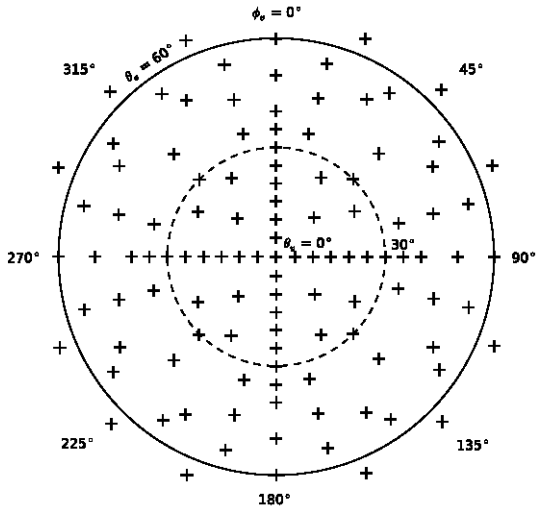

Figure 9. Position and distribution of the sampled observations. The outer circle marks the observation zenith angle of 60° and the inner circle that of 30° of the hemisphere over the target.

Figure 10 shows the approximation of the BRDF at $\lambda = 670$ nm (absorption by chlorophyll) and at $\lambda = 800$ nm (volume scattering) of a winter barley canopy during early stem elongation. This resulting BRDF shows typical characteristics of a BRDF of vegetation canopies such as the hot spot phenomenon (Gerstl 1988, Gerstl and Simmer 1986) and the bowl shape in the near-infrared region (NIR) (among others, Coulson 1966, Gerstl and Simmer 1986, Sandmeier et al. 1998). It is striking that the hot spot appears stronger in the visible region (cf. *figure 10 (a)*) compared to that in the NIR region (cf. *figure 10 (b)*). The reason is that the hot spot is an effect of single scattering occurring in the visible region due to high pigment absorption, while the NIR region is mainly characterized by multiple scattering due to the leaf's internal structure (Sandmeier and Deering 1999). Typically, forward scattering reflectance is lower than backward scattering reflectance due to casting shadows. This effect is independent from wavelength and can be seen on both surfaces shown in *figure 10*. The typical bowl shape in the NIR region is caused by volume scattering, due to multiple scattering within the canopy that affects diffuse radiation illuminating the shady interior of the canopy, decreasing the effect of shadows. The strength of the bowl shape depends on several factors, such as density, LAI and height of the canopy. Another striking feature is the appearance of a local maximum in the visible red region around the nadir point (located in the center of the surface) and of a local minimum in the NIR region around the nadir point. This can be explained as an effect of the nadir view, where the soil background of the canopy is clearly visible in contrast to off-nadir viewings. In this

simulation the soil signal is higher than the vegetation signal in the visible red region causing the local maximum and on the contrary in the NIR region the soil signal is lower than the vegetation signal causing the local minimum.

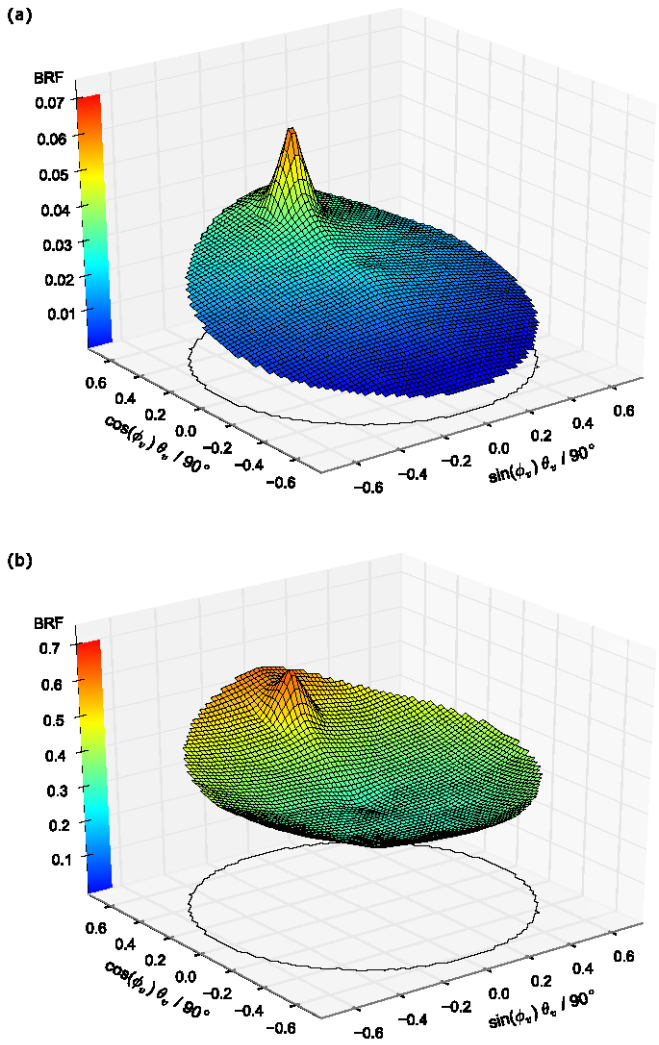

Figure 10. The approximation of the BRDF at (a) λ = 680 nm and at (b) λ = 800 for a representative virtual barley canopy during early stem elongation (BBCH 31, phenological stage 4, LAI=2.5, PC=79%) with a solar zenith angle θ_i = 40°.

4. Conclusion and outlook

This paper presents the description of *HySimCaR*, a spectral, spatial and temporal simulation system that can be used to model the bidirectional canopy reflectance and the BRDF of canopies for three cereal types. Canopy architecture is described by detailed plant representatives linked with spectral information. The plant representatives are built with a structural whole plant simulation tool based on botanical knowledge that is able to describe plant architecture geometrically at different phenological stages. With

the exception of the transmittance of leaves, all the spectral data are natural spectra collected in the field, thereby approximating reality. This is an important fact for complex simulations that ensure the transferability to the actual application.

The nadir bidirectional reflectance of the modeled cereal canopies is computed by using Monte-Carlo ray tracing techniques. The resulting bidirectional canopy reflectance was validated spectrally and structurally for all the modeled cereal types and phenological stages. The validation after both aspects has shown that the modeled cereal canopies were well recreated. Additionally, it was shown that it is possible to generate canopy reflectance with the simulation system comparable to that measured in the field. The interpolation of numerous observed bidirectional canopy reflectance values from different viewing positions enables the modeling of the BRDF of cereal canopies.

This paper focuses on the description of the methodology and its validation. Detailed analyses of different influences on the BRDF using data generated with *HySimCaR* are subject of another paper. Nevertheless, the advantages using the proposed simulation system are manifold:

- *HySimCaR* offers an alternative approach to field measurements to obtain an approximation of the BRDF of cereal canopies. In the field the BRDF of vegetation canopies is approximated by numerous time-consuming measurements with a goniometer (e.g., Huang et al. 2008, Landis and Aber 2007, Sandmeier 2000). Computer based approaches like *HySimCaR* have a great advantage over field measurements, since the conditions for the modeling of the BRDF can be held constant. Thus, it is possible to exclude disturbing effects such as the movement of the sun and the crossing of cirrus clouds from the measurements. Additionally, it is possible to vary any parameter entering the model, e.g. cereal type, phenological stage, soil type, plant density, and illumination conditions. This enables the sampling of a wide variety of scenarios that would not be realizable in the field.
- With *HySimCaR* it is possible to obtain a representative test bench of realistic bidirectional reflectance and BRDF data for analyzing tasks (e.g., analyzing the effects due to plant and canopy structure) or for applications. It enables the development of spectral libraries for any modellable setup that can serve as training data for classification tasks or other applications strengthening the independence of ground truth data. Furthermore, it is possible to improve the results by including off-nadir observations that is particularly in the case of airborne image data of importance because the field of view varies across the flight direction.
- *HySimCaR* supports the development of the derivation of specific correction methods minimizing the influence of illumination and viewing geometry within a single image scene. This is particularly important for data recorded by airborne sensors. Their wide field of view leads to strong spectral variations between single image columns due to varying viewing angles in across track direction. Assessing these influences would greatly support an improved interpretation and quantification of the data.

- Precisely simulated BRDF data are also valuable information for the preparation of new remote sensing missions. These data can serve for the optimization of the instrument design and for the development of new methods for the scientific exploitation of future sensor data.

At the current stage, *HySimCaR* is developed for three important cereal species (wheat, rye and barley). Enlarging the data base of plant models with more species, especially with the most cultivated species maize and rice, is an important future task and will address a broader range of applications. Furthermore, coupling *HySimCaR* with a leaf reflectance model like PROSPECT (Jacquemoud and Baret 1990) would enable to study also the effects of leaf optical properties on canopy bidirectional reflectance and BRDF multitemporal. Summarizing, *HySimCaR* and their future enhancements will be a significant contribution towards the improvement of remote sensing approaches and the retrieval of high quality remote sensing products.

Acknowledgements

EnMAP and the associated research works are funded on behalf of the German Space Administration with resources of the German Federal Ministry of Economic Affairs and Technology. The authors would like to thank the AGRAR GbR Wittbrietzen and the Faculty of Agriculture and Horticulture of the Humboldt-University Berlin for enabling the data collection. They are also grateful to Prof. P. Lewis for providing *drat* and its support. The authors would like to thank the anonymous reviewers for their valuable comments and suggestions to improve the quality of the paper.

References

Bacour, C., 2001, *Contribution à la détermination des paramètres biophysiques des couverts végétaux par inversion de modèles de réflectance : analyses de sensibilité comparatives et configurations optimales*. Thesis (PhD). Université Paris Diderot.

Baghestani, M., Zand, E. and Soufizadeh, S., 2006, Iranian winter wheats (triticum aestivum l.) interference with weeds: II. growth analysis. *Pakistan Journal of Weed Science Research*, 12(3), pp. *131 – 144*.

Barczi, J.-F., de Reffye, P. and Caraglio, Y., 1997, Essai sur lidentification et la mise en oevre des paramètres nécessaires à la simulation d'une architecture végétale: le logiciel AmapSim. *In:* J. Bouchon, P. de Reffye and D. Barthélémy, eds, *Modélisation et simulation de l'architecture des végétaux*. Paris: INRA Editions, pp. *205 – 254*.

Barczi, J.-F., et al., 2008, AmapSim: A structural whole-plant simulator based on botanical knowledge and designed to host external functional models. *Annals of Botany*, 101, pp. *1125 – 1138*.

Barnsley, M.J., Settle, J.J., Cutter, M.A., Lobb, D.R., Teston, F., 2004, The PROBA/CHRIS mission: a low-cost smallsat for hyperspectral multiangle observations of the Earth surface and atmosphere. *IEEE Transactions on Geoscience and Remote Sensing*, 42(7), pp. *1512 – 1520*.

Bégué, A., 1992, Modeling hemispherical and directional radiative fluxes in regular-clumped canopies. *Remote Sensing of Environment*, 40(3), pp. *219 – 230*.

Borel, C. C., Gerstl, S. A. and Powers, B. J., 1991, The radiosity method in optical remote sensing of structured 3-D surfaces. *Remote Sensing of Environment*, 36(1), pp. *13 – 44*.

Bréda, N., 2003, Ground-based measurements of leaf area index: a review of methods, instruments and current controversies. *Perspectives in Experimental Botany*, 54(392), pp. *2403 – 2417*.

Castel, T., Caraglio, Y., Beaudoin, A. and Borge, F., 2001, Using SIR-C SAR data and the AMAP model for forest attributes retrieval and 3-D stand simulation. *Remote Sensing of Environment*, 75(2), pp. *279 – 290*.

Coulson, K., 1966, Effects of reflection properties of natural surfaces in aerial reconnaissance. *Applied Optics*, 5(6), pp. *905 – 917*.

Dauzat, J. and Hautecoeur, O., 1991, Simulation des transferts radiatifs sur maquettes informatiques de couverts végétaux. *In: ESA. Proceedings of the 5th international colloquium. Physical measurements and signatures in remote sensing*. Courchevel, France., pp. *415 – 418*.

de Reffye, P., et al., 1988, Plant models faithful to botanical structure and development. *In: Proceedings of the 15th Annual Conference on Computer Graphics and Interactive Techniques, SIGGRAPH 1988*, pp. *151 – 158*.

Disney, M.I., Lewis, P., and North, P.R.J., 2000, Monte Carlo raytracing in optical canopy reflectance modelling, Remote Sensing Reviews, 18, pp. 163 – 196.

Disney, M., Lewis, P. and Saich, P., 2006, 3D modelling of forest canopy structure for remote sensing simulations in the optical and microwave domains. *Remote Sensing of Environment*, 100, pp. *114 – 132*.

Dosio, G.A., Rey, H., Lecoeur, J., Izquierdo, N.G., Aguirrezábal, L.A., Tardieu, F., Turc, O., 2003, A whole-plant analysis of the dynamics of expansion of individual leaves of two sunflower hybrids. *Journal of Experimental Botany*, 54, pp. *2541 – 2552*.

España, M.L., Baret, F., Aries, F., Chelle, M., Andrieu, B., Prévot, L., 1999, Modeling maize canopy 3D architecture: Application to reflectance simulation. *Ecological Modelling*, 122(1-2), pp. *25 – 43*.

Féret, J.-B., François, C., Asner, G.P., Gitelson, A.A., Martin, R.E., Bidel, L.P.R., Ustin, S.L., le Maire, G., and Jacquemoud, S., 2008, PROSPECT-4 and 5: Advances in the leaf optical properties model separating photosynthetic pigments. *Remote Sensing of Environment*, 112(6), pp. *3030 – 3043*.

Galeazzi, C., Sacchetti, A., Cisbani, A., and Babini, G., 2008, The PRISMA program. *In: IEEE Geoscience and Remote Sensing Symposium, Proceedings of IGARSS*, Boston, MA, USA.

Gao, W., 1993, A simple bidirectional-reflectance model applied to a tall grass canopy. *Remote Sensing of Environment*, 45(2), pp. *209 – 224*.

Gastellu-Etchegorry, J., Demarez, V., Pinel, V., and Zagolski, F., 1996, Modeling radiative transfer in heterogeneous 3-D vegetation canopies. *Remote Sensing of Environment*, 58(2), pp. *131 – 156*.

Gastellu-Etchegorry, J.-P., Martin, E., and Gascon, F., 2004, Dart: A 3D model for simulating satellite images and studying surface radiation budget. *International Journal of Remote Sensing*, 25, pp. 73 – 96.

Gerstl, S., 1988, The angular reflectance signature of the canopy hot spot in the optical regime. *In: Proceedings of the 4th. International Colloquium Spectral Signatures of Objects in Remote Sensing*, Aussois, France, pp. *129 – 132*.

Gerstl, S. and Simmer, C., 1986, Radiation physics and modelling for off-nadir satellite sensing of non-lambertian surfaces. *Remote Sensing of Environment*, 20, pp. *1 – 29*.

Glassner, A., 1989, *An introduction to ray tracing*. 8th ed. Academic Press Ltd.

Goel, N., 1988, Models of vegetation canopy reflectance and their use in the estimation of biophysical parameters from reflectance data. *Remote Sensing Reviews*, 4, pp. *1 - 222*.

Goel, N., Knox, L. and Norman, J., 1991, From artificial to real life: computer simulation of plant growth. *International Journal of General Systems*, 18, pp. *291 - 319*.

Govaerts, Y., and Verstraete, M.M., 1998, Raytran: A Monte Carlo ray tracing model to compute light scattering in three-dimensional heterogeneous media, *IEEE Transactions on Geoscience and Remote Sensing*, 36, pp. 493 – 505.

Hu, B.-G. and Jaeger, M., eds., 2003, *Plant growth modeling and applications*. Beijing: Tsinghua University Press.

Huang W., Wang J., Wang Z., Ma Z., Zhao C., 2008. Winter wheat geometry identification by bidirectional canopy reflected spectrum. *International Journal of Agricultural and Biological Engineering*, 1 (2), pp. *27 – 31*.

Ivanov, N., Boissard, P., Chapron, M., Andrieu, B., 1995, Computer stereo plotting for 3-D reconstruction of a maize canopy. *Agricultural and Forest Meteorology*, 75(1-3), pp. *85 – 102*.

Jacquemoud, S. and Baret, F., 1990, PROSPECT: a model of leaf optical properties spectra. *Remote Sensing of Environment*, 34, pp. *75 – 91*.

Jacquemoud et al., 2009, PROSPECT + SAIL models: A review of use for vegetation characterization. Remote Sensing of Environment, 113(1), pp. *56 – 66*.

Jaeger, M. and de Reffye, P., 1992, Basic concepts of computer simulation of plant growth. *Journal of Biosciences*, 17(3), pp. *275 – 291*.

Kanemasu, E., 1974, Seasonal canopy reflectance patterns of wheat, sorghum, and soybean. *Remote Sensing of Environment*, 3(1), pp. *43 – 47*.

Kirby, E., 2002, Botany of the wheat plant. *In:* B. Curtis, S. Rajaram and H. G. Macpherson, eds, *Bread wheat - Improvement and Production*, *FAO Plant Production and Protection Series*. Rome: Food and Agriculture organization of the United Nations, p. *567*.

Kurth, W., 1994, Morphological models of plant growth: Possibilities and ecological relevance. *Ecological Modelling*, 75 - 76, pp. *299 – 308*.

Kuester, T., 2011, *Modellierung von Getreidebestandsspektren zur Korrektur BRDF-bedingter Einflüsse auf Vegetationsindizes im Rahmen der EnMAP-Mission*. Thesis (PhD), Humboldt-Universität zu Berlin.

Landis, B. and Aber, J., 2007, Low-cost field goniometer for multiangular reflectance measurements. *Emporia State Research Studies*, 44(1), pp. *1 – 6*.

Lewis, P., 1999, Three-dimensional plant modelling for remote sensing simulation studies using the botanical plant modelling system. *Agronomie - Agriculture and Environment*, 19, pp. *185 – 210*.

Li, X. and Strahler, A., 1986, Geometric - optical bidirectional reflectance modeling of a conifer forest canopy. *IEEE Transactions on Geoscience and Remote Sensing*, GE-24(6), pp. *906 – 919*.

Li, X., Strahler, A. and Woodcock, C., 1995, A hybrid geometric optical-radiative transfer approach for modeling albedo and directional reflectance of discontinuous canopies. *IEEE Transactions on Geoscience and Remote Sensing*, 33(2), pp. *466 – 480*.

Lindenmayer, A., 1968, Mathematical models for cellular interaction in development. *Journal of Theoretical Biology*, 18, pp. *280 – 315*.

Luquet, D., Begue, A., Dauzat, J., Nouvellon, Y., Rey, H., 1998, Effect of the vegetation clumping on the BRDF of a semi-arid grassland: Comparison of the SAIL model and ray tracing method applied to a 3D computerized vegetation canopy. *In: IEEE International Geoscience and Remote Sensing Symposium. Proceedings of IGARSS 1998*, Vol. 2, pp. *791 – 793*.

Mialet-Serra, I., Dauzat, J. and Auclair, D., 2001, Using plant architectural models for estimation of radiation transfer in a coconut-based agroforestry system. *Agroforestry Systems*, 53(2), pp. *141 – 149*.

Monteith, J., 1973, *Principles of Environmental Physics*. London: Edward Arnold.

Moulia, B. and Sinoquet, H., 1993, Three - dimensional digitizing systems for plant canopy geometrical structure: a review. *In:* R. Bonhomme, H. Sinoquet and C. Varlet-Grancher, eds, *Crop structure and light micro - climate: characterization and applications, Science Update Series*. Paris: INRA Editions, pp. *183 – 193*.

Mündermann, L., Erasmus, Y., Lane, B., Coen, E., Prusinkiewicz, P., 2005, Quantitative modeling of arabidopsis development. *Plant Physiology*, 139, pp. *960 – 968*.

Myneni, R., Asrar, G. and Gerstl, A., 1990, Radiative transfer in three dimensional leaf canopies. *Transport Theory and Statistical Physics*, 19(3-5), pp. *205 – 250*.

Ni, W., Li, X., Woodcock, C.E., Caetano, M.R., Strahler, A.H., 1999, An analytical hybrid gort model for bidirectional reflectance over discontinuous plant canopies. *IEEE Transactions on Geoscience and Remote Sensing*, 37(2), pp. *987 – 999*.

Nicodemus, F.E., Richmond, J.C., Hsia, J.J., Ginsberg, I.W., Limperis, T., 1977, Geometrical considerations and nomenclature for reflectance. Washington, DC: National Bureau of Standards, US Department of Commerce.

North, P.R.J., 1996, Three-dimensional forest light interaction model using a Monte Carlo method, *IEEE Transactions on Geoscience and Remote Sensing*, 34, pp. *946 – 956*.

Pinty, B., Gobron, N., Widlowski, J.-L., Gerstl, S.A.W., Verstraete, M.M., Antunes, M., Bacour, C., Gascon, F., Gastellu, J.-P., Goel, N., Jacquemoud, S., North, P., Qin, W., Thompson, R., 2001, Radiation transfer model intercomparison (RAMI) exercise. *Journal of Geophysical Research*, 106, pp. *11937 – 11956*.

Prusinkiewicz, P. and Lindenmayer, A., 1990, *The algorithmic beauty of plants*. New York: Springer.

Rey, H., Dauzat, J., Chenu, K., Barczi, J.-F., Dosio, G.A.A., Lecoeur, J., 2008, Using a 3-D virtual sunflower to simulate light capture at organ, plant and plot levels: Contribution of organ interception, impact of heliotropism and analysis of genotypic differences. *Annals of Botany*, 101, pp. *1139 – 1151*.

Saich, P., Lewis, P. and Disney, M., 2003, Biophysical parameter retrieval from forest and crop canopies in the optical and microwave domains using 3D models of canopy structure. *In: IEEE International Geoscience and Remote Sensing Symposium. Proceedings of IGARSS 2003*, Vol. 6, Toulouse, France, pp. *3546 – 3548*.

Saich, P., Lewis, P., Disney, M., Thackrah, G., 2002, Comparison of Hymap/E-SAR data with models for optical reflectance and microwave scattering from vegetation canopies. *In:* A. Wilson, ed., ESA Publications Division, *Proceedings of the Third International Symposium on Retrieval of Bio- and Geophysical Parameters from SAR Data for Land Applications*, Sheffield, UK, pp. *75 – 80*.

Sandmeier, S., 2000. Acquisition of bidirectional reflectance factor data with field goniometers. *Remote Sensing of Environment*, 73(3), pp. *257 – 269*.

Sandmeier, S., and Deering, D., 1999, Structure analysis and classification of boreal forests using airborne hyperspectral BRDF data from ASAS. *Remote Sensing of Environment*, 69(3), pp. *281 – 295*.

Sandmeier, S., Müller, C., Hosgood, B., Andreoli, G., 1998, Physical mechanisms in hyperspectral BRDF data of grass and watercress. *Remote Sensing of Environment*, 66(2), pp. *222 – 233*.

Schaepman-Strub, G., Schaepman, M.E., Painter, T.H., Dangel, S., Martonchik, J.V., 2006, Reflectance quantities in remote sensing – definitions and case studies. *Remote Sensing of Environment*, 103(1), pp. *27 – 42*.

Segl, K., Guanter, L., Rogass, C., Kuester, T., Roessner, S., Kaufmann, H., Sang, B., Mogulsky, V., Hofer, S., 2012, Eetes - the EnMAP end-to-end simulation tool. *IEEE Journal of Selected Topics in Applied Earth Observations and Remote Sensing*, 5(2), pp. *522 – 530*.

Stuffler, T., Kaufmann, H., Hofer, S., Forster, K.P., Schreier, G., Mueller, A., Eckardt, A., Bach, H., Penne, B., Benz, U., Haydn, R., 2007, The EnMAP hyperspectral imager - An advanced optical payload for future applications in Earth observation programmes. *Acta Astronautica*, 61, pp. *115 – 120*.

Suits, G., 1972, The calculation of the directional reflectance of a vegetative canopy. *Remote Sensing of Environment*, 2, pp. *117 – 125*.

Thompson, R. L., and Goel, N.S., 1998, Two models for rapidly calculating bidirectional reflectance: Photon spread (ps) model and statistical photon spread (sps) model, *Remote Sens. Rev.*, 16, pp. *157 – 207*.

Verbrugghe, M. and Cierniewski, J., 1995, A geometrical model of plant bidirectional reflectance. *In: Proceedings of the International Colloquium - Photosynthesis and Remote Sensing*, 28-30 August, 1995, Montpellier, France, pp. *243 – 248*.

Verhoef, W., 1984, Light scattering by leaf layers with application to canopy reflectance modeling: The SAIL model. *Remote Sensing of Environment*, 16(2), pp. *125 – 141*.

White, H.P.,Miller, J.R. and Chen, J.M., 2001, Four-scale linear model for anisotropic reflectance (FLAIR) for plant canopies. I: model description and partial validation. *IEEE Transactions on Geoscience and Remote Sensing*, 39(5), pp. *1072 – 1083.*

Widlowski, J.-L., Lavergne, T., Pinty, B., Verstraete, M.M., Gobron, N., 2006, Rayspread: A virtual laboratory for rapid BRF simulations over 3-D plant canopies. *Computational Methods in Transport, Lecture Notes in Comput. Sci. and Eng. Ser.*, vol. 48, edited by G. Frank, pp. *211 – 231*, Springer, New York.

Widlowski, J.-L., Taberner, M., Pinty, B., Bruniquel-Pinel, V., Disney, M., Fernades, R., Gastellu-Etchegorry, J.-P., Gobron, N., Kuusk, A., Lavergne, T., Leblanc, S., Lewis, P., Martin, E., Mottus, M., North, P., Qin, W., Robustelli, M., Rochdi, N., Ruiloba, R., Soler, C., Thompson, R., Verhoef, W., Verstraete, M., Xie, D., 2007, The third RAdiation transfer Model Intercompariosn (RAMI) exercise: Documenting progress in canopy reflectance models. *Journal of Geophysical Research*, 112, D09111, 28.

Yan, H., Kang, M.Z., de Reffye, P., Dingkuhn, M., 2004, A dynamic, architectural plant model simulating resource-dependent growth, *Anals of Botany*, 93, pp. *591 – 602*.

Zhang, Y., Yu, Q., Liu, C., Jiang, J., Zhang, X., 2004, Estimation of winter wheat evapotranspiration under water stress with two semiempirical approaches. *Agronomy Journal*, 96(1), pp. *159 – 168.*